Collapse of a semiflexible polymer in poor solvent

Alberto Montesi,[1,2] Matteo Pasquali,[1,2,*] and F. C. MacKintosh[2,3]

[1]*Department of Chemical Engineering, Rice University, 6100 Main Street, Houston, Texas 77005, USA*
[2]*The Kavli Institute for Theoretical Physics, University of California, Santa Barbara, California 93106, USA*
[3]*Division of Physics and Astronomy, Vrije Universiteit, 1081 HV Amsterdam, The Netherlands*

We investigate the dynamics and pathways of the collapse of a single, semiflexible polymer in a poor solvent via three-dimensional Brownian Dynamics simulations. An example of this phenomenon is DNA condensation induced by multivalent cations. Earlier work indicates that the collapse of semiflexible polymers generically proceeds via a cascade through metastable racquet-shaped, long-lived intermediates towards the stable torus state. We investigate the rate of decay of uncollapsed states, analyze the preferential pathways of condensation, and describe the likelihood and lifespan of the different metastable states. The simulations are performed with a bead-stiff spring model with excluded volume interaction, bending stiffness, and exponentially decaying attractive potential. The semiflexible chain collapse is studied as a function of the three relevant length scales of the phenomenon, i.e., the total chain length L, the persistence length L_p, and the condensation length $L_0 = \sqrt{k_B T L_p / u_0}$, where u_0 is a measure of the attractive potential per unit length. Two dimensionless ratios, L/L_p and L_0/L_p, suffice to describe the dimensionless decay rate of uncollapsed states, which appears to scale as $(L/L_p)^{1/3}(L_0/L_p)$. The condensation sequence is described in terms of the time series of the well separated energy levels associated with each metastable collapsed state. The collapsed states are described quantitatively through the spatial correlation of tangent vectors along the chain. We also compare the results obtained with a locally inextensible bead-rod chain and with a phantom bead-spring chain. Finally, we show preliminary results on how steady shear flow influences the kinetics of collapse.

I. INTRODUCTION AND MOTIVATION

The conformation of individual polymer chains depends on the solvent properties [1–3]. In good solvent, the monomers effectively repel each other, preferring to be surrounded by solvent. This effect leads to a swollen coil conformation for flexible polymers in good solvent. In poor solvent, conversely, the monomers try to exclude the solvent and effectively attract one another, and a flexible chain forms a compact globule of roughly spherical shape to minimize the contacts between monomers and solvent. The dynamics of the coil-globule transition in flexible chains are well known [4–7] and involve the formation of a pearl necklace and the gradual diffusion of large pearls from the chain ends [8,9].

An early theoretical picture of the phenomenon predicted the initial formation of a dense, uniform, sausage-like shape aggregate, which in a second stage forms a globule, driven by surface area minimization [4]. The first experimental evidence of a two-stage kinetic was later obtained using a thin capillary tube cell for dynamic light scattering measurements [8]. More recently, simulations showed that capillary instability prevents the formation of such sausage-like shapes and that the condensation pathway actually involves an initial fast crumpling of the unknotted polymer chain, with the formation of pearls of collapsed, dense phase connected by uncollapsed bridges, and a subsequent slow rearrangement of these pearls to form a compact globule [6,9]. Each stage is characterized by a length scale, and by a time scale increasing with the relevant length scale. The pearling stage in-

volves only local rearrangement of the chain configurations, while the dimensions and configurations of the whole chain are weakly modified. The pearls then grow attracting monomers from the bridges, which become increasingly stretched and then shrink as the collapse proceeds. Eventually, the pearls come into contact, coalescing into a single globule.

Many polymers, however, exhibit substantial bending stiffness, i.e., they are semiflexible, and they collapse in poor solvent towards very different equilibrium states, and following different kinetics. Semiflexible polymers can be described by the wormlike chain model; examples include biopolymers (such as F-actin, DNA, and xanthan) as well as synthetic polymers (such as PPTA and PBO) used for production of high-performance fibers (e.g., Kevlar[TM] and Zylon[TM]). Such polymers form open, extended structures in good solvents. In poor solvent, the effective self-affinity of the chain leads to chain collapse. The collapsed state configurations and the pathways to their formation are the result of the interplay between two opposing forces: the bending force related to the chain stiffness and the attractive force due to the poor solvency of the environment.

A compact globule is energetically unfavorable for semiflexible polymers because it involves bending over short length scales. The collapsed ground state is instead a torus, which reduces the monomer-solvent contacts without causing excessive bending penalty, i.e., ensuring that the chain is still roughly straight on short length scales. Theoretical analysis [10,11], Monte Carlo simulations [12], and experimental evidence [13,14] have detailed the stability, the features, and the packing of the collapsed tori. The dynamics of the collapse of wormlike chains in poor solvent have been investigated more recently [15–17], strongly suggesting a

*Electronic address: mp@rice.edu

possible generic pathway for the collapse of semiflexible polymers, featuring a series of long-lived, partially collapsed, racquet-shaped intermediate states, before the eventual collapse to a torus. Such intermediate states form an energetically driven cascade of increasingly compact conformations with sharp transitions between their energy levels.

The dynamics of collapse of semiflexible molecules is relevant for understanding DNA condensation. DNA frequently forms condensed structures *in vivo*, e.g., in DNA replication, viral transfection, and compaction within sperm heads and nucleosomes [14]. Controllable *in vitro* DNA condensation is involved in nonviral gene therapy—which is used in the treatment of various kinds of disease, including cancer—for packaging in, and transfection from gene delivery vehicles. Multivalent cations, in particular polyamines, have been used to induce condensation *in vitro*, showing that condensed DNA exists in toroidal and rodlike structures. Polyamines present ubiquitously in living cells in millimolar concentrations (e.g., putrescine and spermidine) are also believed to induce condensation *in vivo* [18]. A better understanding of the dynamics of condensation would lead to improvements in gene delivery technology, as it may help defining the best conditions and protocols to obtain DNA condensation.

In the present work, we verify previous hypotheses [15] of the suggested pathway for the collapse of semiflexible polymers and further explore the effect of the relevant length scales on the phenomenon. The natural length scale for the polymer stiffness is its intrinsic persistence length L_p, defined as the ratio of the bending stiffness κ to the thermal energy $k_B T$, which represents the length along the chain for which tangent vectors remain correlated in a theta solvent, i.e., in absence of energetic (attractive or repulsive) interactions between chain and solvent. In a poor solvent, the balance between intrachain attractive forces and bending forces can be considered in terms of the so-called "condensation length" $L_0 = \sqrt{kTL_p/u_0}$, where u_0 is the value of the attractive potential per unit length. We choose as time scale for the collapse event the rotational diffusion time of a perfectly rigid rod with $L = L_p$, $\tau_{\mathrm{rot},L_p} = \zeta L_p^3/(72 k_B T)$, where ζ is the transverse friction coefficient [19]. Therefore we use τ_{rot,L_p} as unit of time and $k_B T$ as unit of energy in presenting all the results of the present work. We investigate the sequences and the likelihood of different collapsed structures formed at various solvent quality (described by u_0) and chain stiffness.

II. SIMULATION DETAILS

The dynamics of the continuous wormlike chain are described by an inertialess Langevin equation:

$$\zeta \cdot \left\{ \frac{\partial \mathbf{r}}{\partial t} - \dot{\boldsymbol{\gamma}} \cdot \mathbf{r} \right\} = -\frac{\delta U}{\delta \mathbf{r}} + \boldsymbol{\eta}. \qquad (1)$$

Equation (1) balances the hydrodynamic force exerted on the chain by the surrounding fluid with the force due to the global potential acting on the chain $U = U_{\mathrm{bend}} + U_{\mathrm{conn}} + U_{\mathrm{solv}}$, and the Brownian force per unit length $\boldsymbol{\eta}$, with correlations $\langle \boldsymbol{\eta}(s,t) \boldsymbol{\eta}(s',t') \rangle = 2 k_B T \zeta \delta(t-t') \delta(s-s')$.

$U_{\mathrm{bend}} = kTL_p \int_0^L ds\, \partial \mathbf{u}(s)/\partial s$ is the bending potential related to the chain stiffness, U_{conn} is the connector potential, U_{solv} describes the monomer-monomer interaction, and the Brownian term accounts for the rate of fluctuating momentum transfer due to the random collisions of small solvent particles with the chain.

The potential U_{solv} chosen to account for the effect of poor solvent is an exponential attractive potential with an excluded volume repulsive term:

$$U_{\mathrm{solv}} = -\int ds \int ds'\, \tilde{u}_0 \exp\left(-\frac{|\mathbf{r}(s) - \mathbf{r}(s')|}{R_{\mathrm{attr}}} \right)$$
$$+ \int ds \int ds'\, \tilde{u}_0 \left(\frac{\sigma}{|\mathbf{r}(s) - \mathbf{r}(s')|} \right)^{12}, \qquad (2)$$

where $\tilde{u}_0$ defines the depth of the potential well, R_{attr} is the range of the attractive forces, and σ is the radius of the excluded volume region. With this potential, $u_0 = R_{\mathrm{attr}} \tilde{u}_0$. Different choices for the shape of the potential should not change the stable and metastable configurations for the wormlike chain in poor solvent, whereas they modify the actual value of the condensation length L_0 and they may alter the speed and the dynamics of the collapse. Our choice of the exponential potential is related to the physics of the condensation phenomenon. DNA and polyelectrolytes collapse because of charge inversion and counterion induced attraction [20]. The attractive forces are therefore due to highly screened electrostatic charges, which typically show an exponential decay, mimicked by the potential selected in this work.

The Brownian Dynamics code used in this work solves in dimensionless, discretized form the Langevin equation of motion of a linear wormlike chain of N beads with positions $\mathbf{R}_1, \ldots, \mathbf{R}_N$, connected by $N-1$ connectors of equilibrium length $a \equiv L/(N-1)$ with unit tangent vectors $\mathbf{u}_i \equiv (\mathbf{R}_{i+1} - \mathbf{R}_i)/a$. For most of the simulations reported in this work, we use quadratic springs as connectors, with a force constant equal to $100\ kT/a^2$, which ensures a small variation of the connectors' length. This choice allows for longer time steps without interfering with the spring relaxation time. We use a midstep algorithm [21] to compute the bead trajectories generated by the equation of motion

$$\zeta_b \left\{ \frac{d\mathbf{R}_i}{dt} - \dot{\boldsymbol{\gamma}} \cdot \mathbf{R}_i \right\} = \mathbf{F}_i = \mathbf{F}_i^{\mathrm{bend}} + \mathbf{F}_i^{\mathrm{elast}} + \mathbf{F}_i^{\mathrm{solv}} + \mathbf{F}_i^{\mathrm{rand}}. \quad (3)$$

Here, $\zeta_b = \zeta a$ is a bead friction coefficient, the bending force is

$$\mathbf{F}_i^{\mathrm{bend}} = \kappa/a \sum_{j=2}^{N-1} \partial(\mathbf{u}_j \cdot \mathbf{u}_{j-1})/\partial \mathbf{R}_i, \qquad (4)$$

the elastic force due to the spring is

$$\mathbf{F}_i^{\mathrm{elast}} = H[(|\mathbf{R}_i - \mathbf{R}_{i-1}| - a)\mathbf{u}_{i-1}$$
$$- (|\mathbf{R}_{i+1} - \mathbf{R}_i| - a)\mathbf{u}_i], \qquad (5)$$

the potential force related to the effective interactions between the beads of the chain, repulsive within the hard core, attractive at short distance is

$$\mathbf{F}_i^{\text{solv}} = \widetilde{u}_0 \sum_{j \neq i} \left[\frac{\exp\left(-\frac{|\Delta\mathbf{R}_{ij}|}{R_{\text{attr}}}\right)}{R_{\text{attr}}} - \frac{12\sigma^{12}}{|\Delta\mathbf{R}_{ij}|^{13}} \right] \frac{\Delta\mathbf{R}_{ij}}{|\Delta\mathbf{R}_{ij}|}, \quad (6)$$

where $\Delta\mathbf{R}_{ij} = \mathbf{R}_i - \mathbf{R}_j$, and the random force is $\mathbf{F}_i^{\text{rand}}$.

Another relevant issue in the simulations is the accurate description of the high curvature of the collapsed states. For a fixed level of arclength discretization, the computational error in the discretized wormlike chain model grows as the chain curvature increases. To achieve an accurate representation of highly curved states characteristic of raquet heads and tori (see Sec. III below) a sufficiently large number of connectors within the characteristic length scale of the collapsed structure is needed. The typical size of the tori and of the racquet heads are of the same order of magnitude of L_p. In the simulation conditions examined here, we found that using 20 connectors per L_p yields an accurate description of chain curvature.

We also performed simulations with a bead-rod model [22,23], which ensures local inextensibility of the wormlike chain. The computational cost for this model is, however, significantly higher (~ 10–50 times) than that for a bead-spring chain model, mainly because a smaller time step is required for convergence. While performing most of the simulations using the bead-spring model, we compared the results for few conditions with the bead-rod model, as discussed in Sec. III D. In that section we also compare some of the results with that obtained using a bead-spring phantom chain, i.e., without excluded volume interactions.

For simplicity, we use isotropic drag in the simulations, and we neglect hydrodynamic interactions between segments of the chain. Including such interactions would likely give minor corrections to the evaluation of the time scales of the phenomena, but it would not change the kinetic pathways and the lifetimes of the intermediate states, because at the beginning of the simulations the chains are locally straight, and after the collapse the hydrodynamic interactions would be dominated by the attractive forces.

III. RESULTS

This section is organized as follows: Sec. III A reports qualitatively the results of our simulations, describing the various possible intermediate configurations and the typical pathways. Section III B presents a more quantitative description of the collapsed states in terms of the correlation function between tangent vectors along the chain and of the energy levels associated with each different collapsed state, which confirm that the toroid is the stable configuration, and show how the collapse proceeds through a cascade of subsequently more energetically favorable metastable states, the various multiple-heads racquets shapes, as predicted from theory [24]. The decay rate of the number of uncollapsed states is investigated as a function of a proper combination of L, L_0, and L_p in Sec. III C, together with a statistical analysis
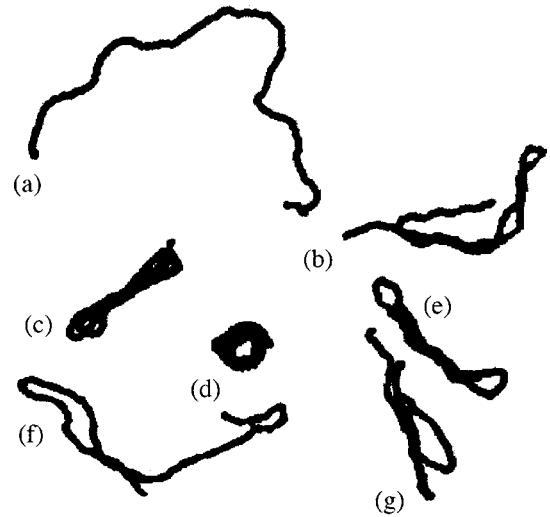

FIG. 1. Typical configurations of an ensemble of collapsing chains at an intermediate time ($L/L_p = 8$, $u_0 = 1.25 kT/a$).

of the preferred collapsed configurations. Sec. III D provides a comparison between the results obtained with the different computational models (phantom chain and bead-rod chain). Some preliminary results of the effect of shear flow on the kinetics and pathways of collapse are presented in Sec. III E.

A. Molecule configurations and collapse pathways

Figure 1 shows a typical snapshot of an ensemble of semiflexible chains during collapse. The 3D structures of the molecules are shown here as 2D projections on a convenient plane. At a given time molecules coexist in different configurations, from completely uncollapsed [molecule (a)], to partially collapsed [molecules (b), (f), and (g)], to higher order racquet [molecules (c) and (e)], to torus [molecule (d)].

The fraction of collapsed molecules increases monotonically with time, confirming that collapsed states are energetically favorable in a bad solvent. Many other ensembles with different values of L/L_p and L_0/L_p show a similar behavior. However, if the attractive forces are not strong enough or the bending stiffness is too high there is no evidence of collapse and the open conformations persist in time. As already observed in [15], a collapse sequence can evolve following two different generic patterns. The first pattern involves the direct formation of a torus from the open conformation, when the two ends of the chain meet while the tangent vectors are locally parallel and pointing in the same direction ($\mathbf{u}_1 \cdot \mathbf{u}_N \approx 1$). In this instance, the chain collapses without formation of any intermediate, the end to end distance drops quickly to a value of the order of the torus dimension, and then fluctuates as the chain keeps folding into the final structure. Meanwhile the total energy of the chain keeps decreasing monotonically until it reaches the equilibrium value. Conversely, the second pattern involves the formation of intermediate metastable states: initially a single-headed racquet which folds quickly into a short-lived, 3-head racquet configuration, and then rearranges as a toroid via a subsequent folding. Figure 2 shows the two different pathways. We no-
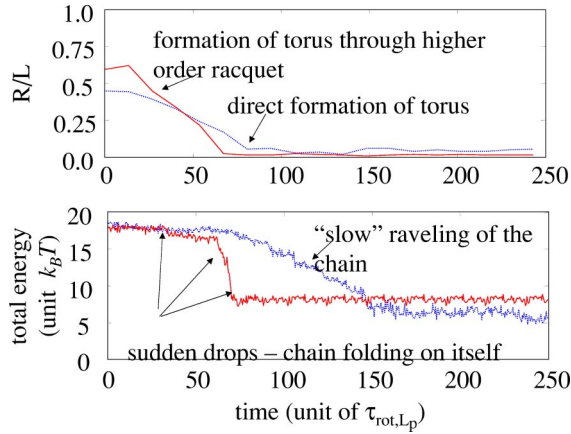
FIG. 2. (Color online) Comparison between time series of end to end distance R and total energy for direct formation of toroid and formation through intermediate states.

tice here that the direct formation of a torus is a more unlikely pattern in 3D—and in fact observed with scarce frequency—than in 2D. Whereas in 2D the relative orientation of the two ends is described by a single angle, two angles are required in 3D and both need to be close to 2π for the direct formation of a torus to take place; therefore, most of the chains initially form a single headed racquet, as described below [25].

The time evolution of the total energy of an ensemble of collapsing chains is shown in Fig. 3. The total energy U of the chain during collapse is defined as the sum of the bending energy U_{bend} and the interaction energy along the chain U_{solv}. In the discretized form,

$$U = kTL_p \sum_{i=1}^{N-2} \cos^2 \theta_i + \sum_{j=1}^{N} \sum_{k=j+1}^{N} u_{\text{solv},jk}, \qquad (7)$$

where θ_i is the bond angle and $u_{\text{solv},jk}$ is the interaction energy evaluated between the beads j and k along the chain.

The time series in Fig. 3 reports most of the possible evolutions observed in our simulations. Few molecules re-

main in the uncollapsed states for the whole duration of the run, equivalent to $250\tau_{\text{rot},L_p}$. For these molecules, the thermal fluctuations never lead two branches of the chain close enough together to initiate the collapse. The other molecules typically reach lower energy states by collapsing in sequentially higher order metastable conformations. The energy levels for each racquet-head shape of increasing order are well separated, and there is a rather large gap from the highest order racquet observed (sixth order) and the stable tori, as expected from theory [24]. It is interesting to compare the actual values of the energy levels obtained in these simulations with those calculated using the theoretical approach.

Schnurr *et al.* [24] obtained the conformational energies of the intermediate racquet states in the absence of thermal fluctuations, relating the annealed shapes to a particular case of Euler's elastica. In their calculations, the relative energetic advantage for segments of the chain to bundle has been evaluated expressing the energy as a surface tension Γ of solvent-exposed sites. For the simulation condition of the data reported in Fig. 3 we get the two sequences of relative energies (theoretical and from simulations) reported in Table I. In both cases, the energy of a straight, uncollapsed chain is set to 1, and we report the energy of the collapsed configurations relative to this one. We note that there is a very good agreement for open chain, 1-head, 2-heads, and 3-heads racquets, whereas the simulation results show lower energy levels for higher order racquets. The reason for these discrepancies, substantial for the more compact conformations, may lie in the finite range of the attractive potential in the simulations. While the theoretical calculation using surface tension accounts only for the local coverage of the filament cross section, the finite range in the simulations allows for next-nearest neighbor interactions, leading to higher stabilization for tighter structures (where each bead has more numerous next-nearest neighbors).

Most of the chains initially form a single head racquet: after the first monomer-monomer contact and the formation of the racquet head, the two sides of the chain tend to become parallel and form a neck region, which ensures the
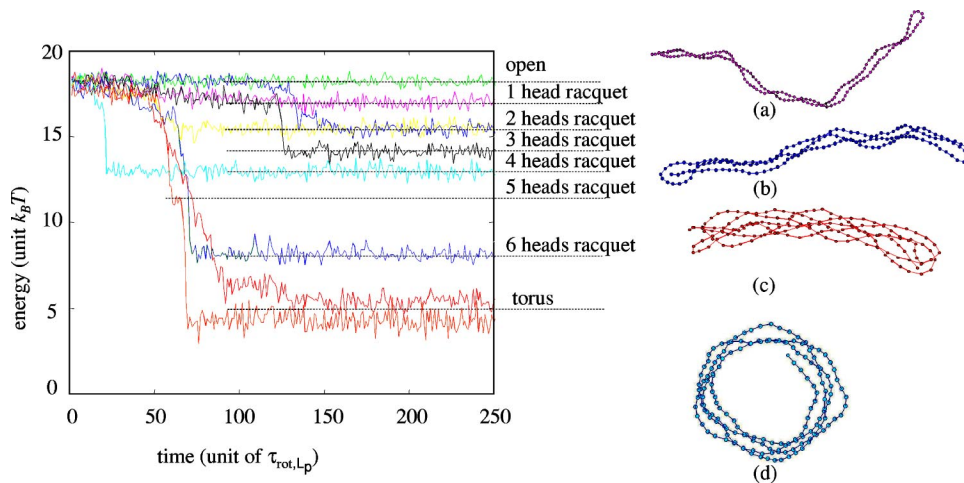

FIG. 3. (Color online) Time series of total energy for an ensemble of molecules, with labels of the corresponding configurations and actual shape of (a) 1 head, (b) 2 heads, (c) 5 heads racquets, and (d) torus.

TABLE I. Comparison between the energy level of the metastable condensed states from theory [24] and present simulations ($L/L_p = 8.0$, $L/L_0 = 65.3$).

Conformational energy (kT)	Theory	Simulation
open chain	1.0	1.0
1-head racquet	0.86	0.87
2-heads racquet	0.75	0.79
3-heads racquet	0.71	0.73
4-heads racquet	0.70	0.66
5-heads racquet	0.68	0.57
6-heads racquet	0.65	0.42

maximum number of monomer-monomer contacts without increasing the bending penalty. The molecules then fold again on themselves, forming higher order shapes. Depending on how the molecule folds back on itself, the next configuration can be a 2-heads or a 3-heads racquet shape. Figure 3 shows examples of both pathways. Successive folding leads to higher order racquets. The transition between each single metastable conformation is very rapid and driven by the deterministic attractive and bending forces. In contrast, the initiating event for each successive collapse is related to the Brownian motion of the molecule, and therefore the time interval between folding events is completely random for the simulations that we have performed. In the simulations of longer chains ($L = 10L_p$) we observe combinations of the conformational elements described above, e.g., chains partially folded in a racquet shape at one end while still uncollapsed at the other. Those conformations have intermediate energies between the well-defined levels corresponding to racquets and tori and quickly disappear in favor of more compact and ordered structures. In contrast, the metastable high order racquets are extremely long-lived, and the energetic barrier for reaching the equilibrium shape is of the order of several k_BT. While the partial unfolding of a torus in a racquet is never observed, simulations show the formation of a torus via metastable configurations, and this, together with the lower total energy shown by the torus (see Fig. 3), confirms once more that the latter is the equilibrium configuration.

B. Quantitative description of collapsed states

The configurations and the shapes of semiflexible molecules in bad solvent can be studied through direct visualization of the collapsing chain. While this method is a valuable way to gather information on the kinetics and pathways of collapse, it is time-consuming and not quantitative. We therefore define a spatial correlation matrix **M** to analyze in a more systematic way the collapsed shapes. The elements of **M** are defined as $M_{ij} = \mathbf{u}_i \cdot \mathbf{u}_j$. With this definition, **M** is symmetric; a perfectly straight rod has $M_{ij} \equiv 1 \ \forall i,j$, as all the connecting normalized vectors have the same direction and orientation. An uncollapsed semiflexible chain with persistence length L_p will have $M_{ii} \equiv 1$, while the off-diagonal terms M_{ij} would be smaller and decaying exponentially with the distance along the chain between the connectors i and j.

When the chain collapses, the actual shape assumed by the molecule can be inferred from the spatial correlation between connectors. The spatial correlation matrix for a single head racquet, for example, will be a block matrix: one block will show values close to 1, corresponding to the almost straight filament in the neck of the racquet, followed by a region with rapidly decreasing values from 1 to -1—the racquet head—and by another block with values close to -1, indicating the other filament of the neck, with the same direction but opposite orientation.

The spatial correlation matrix can be simplified into a spatial covariogram for the molecule. The covariogram is a standard statistical measure of spatial covariance as a function of distance [26], and is defined as

$$C(h) = 1/N(h) \sum_{j=1}^{N} \sum_{i=1}^{N} \{Z_i - \mu\}\{Z_j - \mu\}, \qquad (8)$$

where h is the distance (in time or in space) between the observations Z_i and Z_j, $N(h)$ is the number of observations at a distance h, and μ is the expected average value of the observation. In the present analysis, for each molecule we construct the spatial covariogram C_{sp} assuming $Z_i = \mathbf{u}_i$ and $\mu = \vec{0}$. We therefore obtain a scalar function of the distance along the chain s, bounded between $+1$ and -1, which contains all the relevant information about the shape of the molecule.

Figure 4 shows three relevant examples of this type of analysis: the actual shape of the semiflexible molecules is shown together with the spatial correlation matrix and the spatial covariogram. For a uncollapsed chain [Fig. 4(a)], the matrix shows randomly alternating regions of positive and negative correlation along the length of the chain, corresponding to the typical open configuration of a semiflexible chain in good solvent. The corresponding covariogram shows how the connectors correlation decays from 1 to values around 0 along the length of the chain; the decay is exponential at short distances and related to the stiffness of the chain, i.e., $C_{sp} = \exp(-s/L_p)$. At longer distances, the correlation randomly fluctuates between negative and positive values. As shown in Fig. 4, a single exponential curve with the theoretical coefficient $-1/L_p$ fits very well the spatial covariogram of the open chain, thus confirming the validity of this quantitative analysis.

For a racquet shape with multiple heads, **M** has a structure of alternating blocks with strong positive and strong negative correlation, as shown in Fig. 4(b). The five straight filaments in the neck of the racquet correspond to these five blocks in the matrix; the size of the blocks is approximately the same and indicates the length of the racquet neck. The covariogram shows four zero-crossings, each corresponding to a head of the racquet, and can be fitted quite accurately with a fourth order harmonic; the parameters of this fit are related to the curvature of the racquet heads. From the analysis of the covariogram only, we can extract: (1) the number of heads in the racquet, which is equal to the number of zero-crossing of the covariogram. This relationship can be easily understood recalling that the tangent vector at the edge
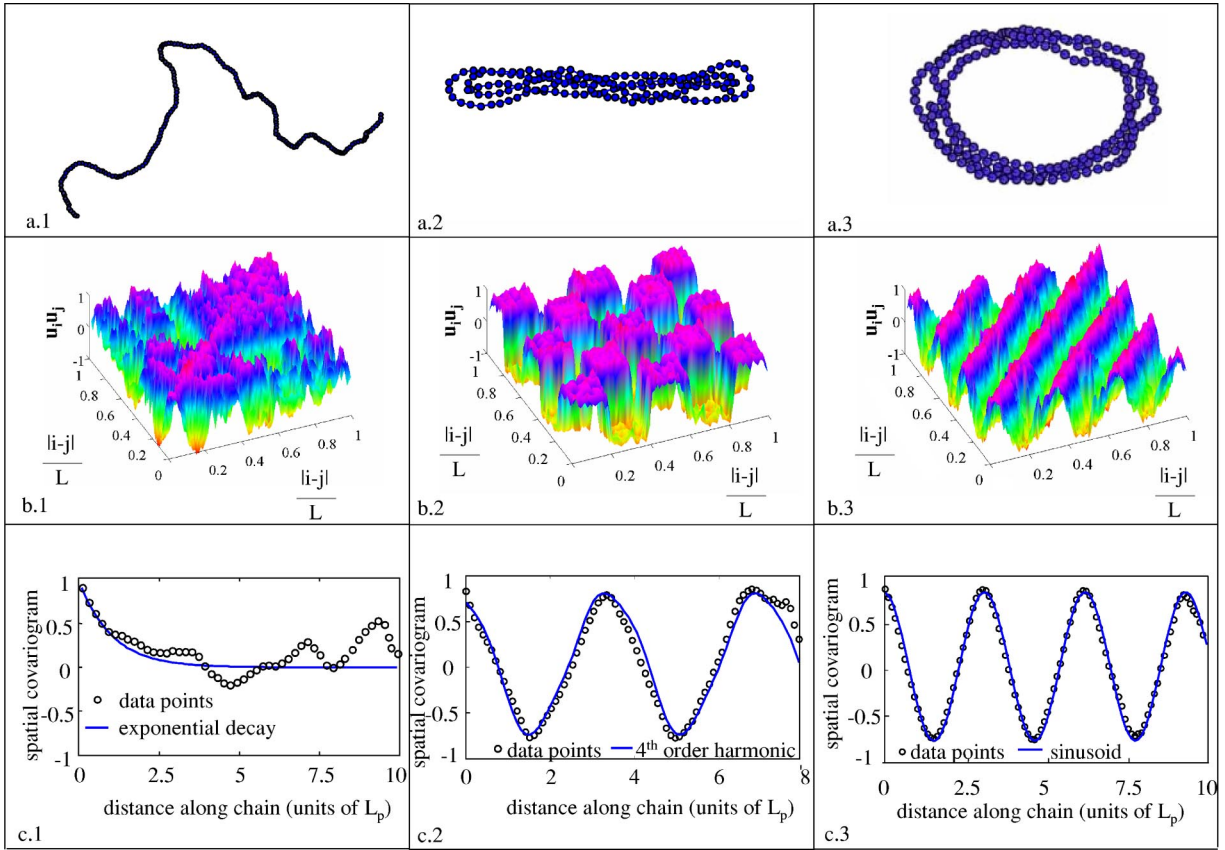
FIG. 4. (Color online) (a) Actual shape, (b) correlation matrix, and (c) spatial covariogram (with fitting curve) for (1) an uncollapsed molecule, (2) a metastable racquet-head shape, and (3) a stable torus.

of the head is perpendicular to the tangent along the neck; and (2) the size of the collapsed molecule, from the distance between two subsequent zero-crossings. In the collapse configuration in Fig. 4(a.2), for example, the length of the 4-heads racquet can be correctly estimated from the covariogram to be about $2 L_p$.

For a torus, the spatial correlation matrix appears completely different [Fig. 4(c)], showing a structure with diagonal bands. In fact, the correlation between pairs of connectors at the same distance is the same, regardless of their position along the chain; this translates into bands along the diagonals of the matrix. The distance between a diagonal with values close to 1 and one with values close to -1 corresponds to the diameter of the collapsed torus. The same information can be extracted from the covariogram, which is a perfect sinusoid, instead of a higher order harmonic function: the period of the sinusoidal function corresponds to π times the diameter of the torus, and the number of complete periods in along the chain indicates the number of loops formed by the collapsed molecule. Again, from the covariogram alone we can derive (1) the number of loops formed by the torus, equal to half of the number of zero-crossing and (2) the size of the collapsed chain, which is in the case of Fig. 4(a.3) equal to roughly $1.5 L_p$.

C. Kinetics of collapse

The fraction of collapsed semiflexible molecules in a bad solvent increases monotonically with time, as already stated.

We have studied the effect of the relevant length scales of the phenomenon, L_p, L_0, and L, on the kinetics of this collapse. By systematically varying the total length of the chain ($L = 3L_p$, $5L_p$, $8L_p$, and $10L_p$), as well as the strength ($\tilde{u}_0 = 0.25kT/a^2$, $0.5kT/a^2$, and $1kT/a^2$) and the range ($R_{attr} = 5/40L_p$ and $1/6L_p$) of the attractive forces, we have explored the effect of these parameters on the decay rate of uncollapsed molecules. We define the time to collapse t_{coll} as the time required by the molecule to form the first metastable collapsed structure. We obtain from simulations the average value of t_{coll} in an ensemble of collapsing chain under each condition, normalized with τ_{rot,L_p}. The inverse of t_{coll} is taken as a measure of the decay rate D_{coll} of uncollapsed molecules. The distribution of the times to collapse follows the expected lognormal distribution, typical of such dynamical processes, with a peak close to the average value and a long tail, as shown in Fig. 5.

At a given value of L/L_p, the decay rate increases, i.e., the molecules collapse faster, for decreasing values of L_0, i.e., for increasing values of u_0. Similarly, the decay rate increases for longer chains at a given value of the attractive potential and persistence length. We can collapse the values of D_{coll} on a single curve as a function of a proper combination of the two dimensionless ratios, L/L_p and L_0/L_p, $(L/L_p)^{1/3}(L_p/L_0)$. Figure 6 shows the mastercurve for the decay rate.

Table II reports the statistics of chains conformations for different values of L/L_p at two different times, i.e., $t1$
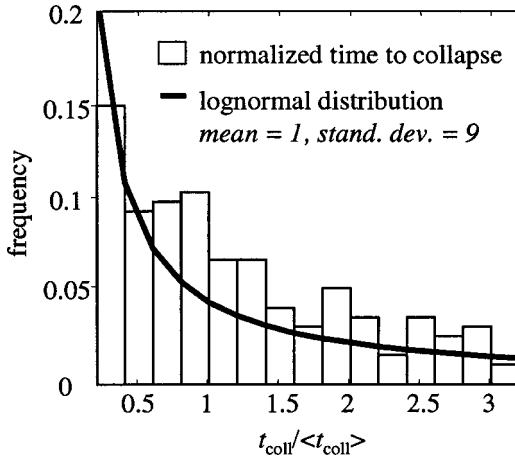
FIG. 5. Normalized collapse time distribution for all the simulation conditions.

FIG. 6. (Color online) Masterplot of the decay rate of uncollapsed molecules.

$=100\tau_{\mathrm{rot},L_p}$ and $t2=200\tau_{\mathrm{rot},L_p}$. At $t1$, the single head racquet is a conformation much more likely than the torus for all the explored values of L/L_p. This confirms that the direct formation of a torus is an unlikely event, as discussed in Sec. III A, and most of the chains collapse through a sequence of folding events. At $t2$, the percentage of molecules in the 1-head racquet configuration does not vary substantially with respect to $t1$, because while uncollapsed molecules fold to form new 1-head racquets, some of these configurations further collapse in higher order metastable racquets and stable tori. The number of chains collapsed in tori or multiple head racquets monotonically increases within the observed span of time. For shorter chains the likelihood of tori and multiple racquets is similar, while the metastable states seem to be initially more favorable for longer chains ($L/L_p=8$ and $L/L_p=10$). Overall, the results show that the intermediates conformations in the collapse phenomenon are extremely long-lived: only 8.4% of the simulated chain has reached the equilibrium, torus state after $200\tau_{\mathrm{rot},L_p}$.

D. Comparison of different computational models

We have performed simulations of collapsing chains with different computational models in order to verify the results obtained and the appropriateness of the model chosen. In particular, we have performed simulations with a bead-rod model, where the chain connectors are rigid rods rather than a stiff elastic spring. As noted in Sec. II, the bead-rod model
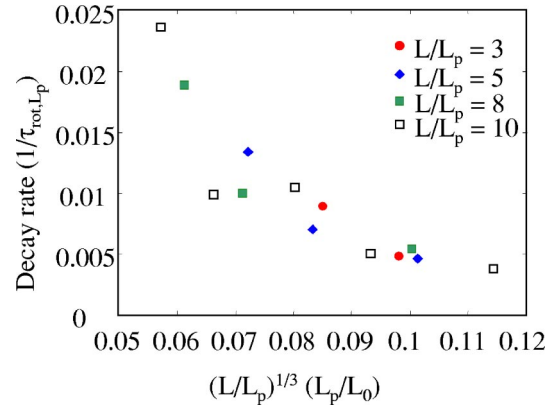
is a constrained model which ensures local inextensibility of the chain, but is computationally more expensive, due to more stringent time step requirements for convergence. While local inextensibility is fundamental when analyzing the polymer contribution to the stress tensor [22], its effect on the pathways and dynamics of collapse is less relevant, as confirmed by our results. In fact, we observe qualitatively similar pathways to collapse in the simulations performed with the bead-rod model. The preferred pathway includes the formation of metastable racquet shapes, similarly to what was observed in the bead-spring simulations. The kinetics of the collapse are slower for the locally inextensible model; we believe that this is due to how the constraints are imposed, i.e., by projecting the random forces onto the constraints, and therefore not allowing any fluctuations along the chain. A more detailed comparison between the collapse kinetics in the two models is prevented by the high computational cost of simulating the constrained system.

We also perform simulations with a phantom bead-spring chain, i.e., a chain with no repulsive hard core. Once more, we find that the dynamics of collapse are qualitatively the same, although the actual shapes of the tori and of the racquets formed by the phantom chain are slightly different. The absence of hard core repulsion allows in fact for tighter structures, as shown in Fig. 7. In particular, in the metastable multiple racquets the neck for phantom chains appears much narrower than for the chains where excluded volume interactions are taken into account, while it is noticeable that the shape and the curvature of the racquet head appears unchanged. The traces in time of the energy level for the phan-

TABLE II. Statistics of chain conformations for different L/L_p at $t1=100\tau_{\mathrm{rot},L_p}$ and $t2=200\tau_{\mathrm{rot},L_p}$ (percent values).

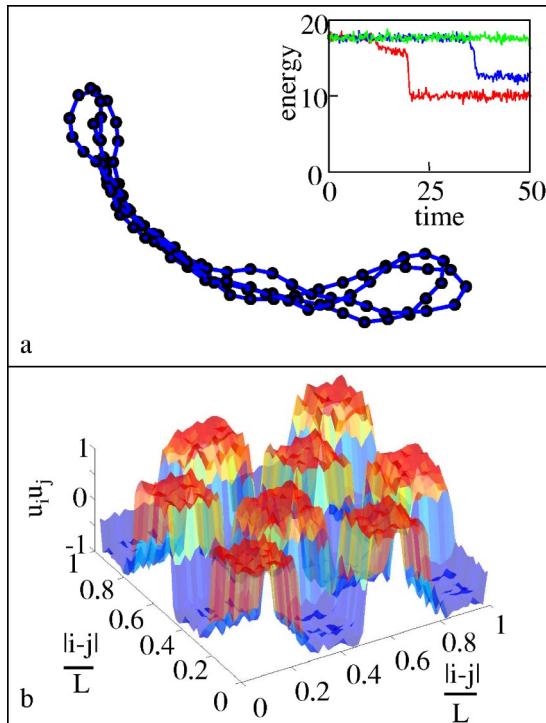| Conformation | $L/L_p=3$ | | $L/L_p=5$ | | $L/L_p=8$ | | $L/L_p=10$ | |
	$t1$	$t2$	$t1$	$t2$	$t1$	$t2$	$t1$	$t2$
open chain	62.0	43.2	48.0	30.0	43.3	36.6	49.0	36.8
single head	31.0	43.2	36.0	42.5	33.4	30.0	24.5	23.7
multiple heads	3.5	6.7	8.0	15.0	20.0	26.7	20.4	31.6
torus	3.5	7.9	8.0	12.5	3.4	6.7	6.1	7.9

FIG. 7. (Color online) (a) Metastable racquet-headed state for a phantom chain and (b) corresponding correlation matrix. Inset in (a): energy traces in time for collapsing phantom chains.

tom chain show the features already discussed in Sec. III A: well-defined energy states corresponding to metastable structures, with rapid transitions between them (see Fig. 7, inset). However, the average life of metastable states appear slightly shorter than in the complete model: intuitively, this is due to the wider range of motion of the phantom chain, which permits folding paths otherwise prevented by the excluded volume interactions.

E. Effect of shear flow

We discuss here the results of some preliminary work on the effects of steady shear flow on the collapse dynamics of semiflexible chains. In particular we monitor the decay rate D_{coll} at different flow strengths, and we compare the pathways of collapse with those at equilibrium. Flexible chains expand in shear flow, i.e., the average end to end distance increases while the molecules tend to orient with the flow; the effect of the flow is therefore counteracting that of the attractive forces, which tend to form compact globuli. Stiff semiflexible chains, with $L_p \geq L$ shrink in shear flow, due to a buckling instability [27]; such rigid chains, however, would not collapse to form tori and multiple racquets in bad solvent, as the open, rodlike shape is stable at equilibrium [24]. In this work, we consider the collapse of less stiff semiflexible molecules: is not clear *a priori* what to expect for the collapse dynamics under shear flow.

We use a freely draining model for the chain under shear. While hydrodynamic interactions are crucial in describing the dynamics of flexible chains in shear flow [28], their effect is far less relevant in a semiflexible chain. For flexible
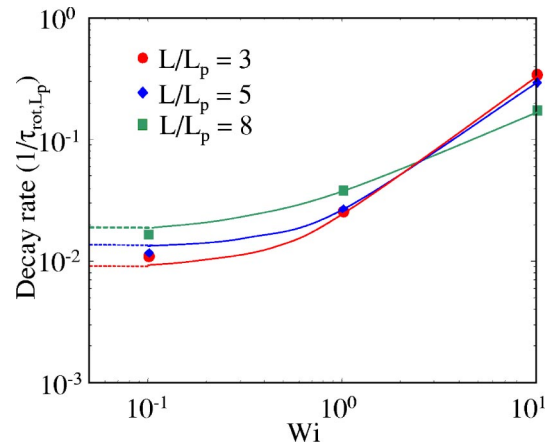

FIG. 8. (Color online) Plot of the decay rate D_{coll} vs Wi for $L/L_p = 3,5,8$, $\tilde{u}_0 = 1kT$, and $R_{attr} = 10/3$.

chains in fact, different segments of the chain contribute very differently to the viscous drag: the segments in the core of the polymer coil—or globule in the poor solvent conditions—are partially shielded from the flow, thus reducing the overall viscous drag. For a stiffer chain, however, this effect is negligible, because locally the molecule is straight and the shielding effect from the other part of the chain is highly reduced. The appropriate approach therefore is using slender body hydrodynamics; in this context, the friction tensor can be written as $\zeta = \zeta_\parallel uu + \zeta(I - uu)$. For a slender rod, $\zeta_\parallel = 0.5\zeta$. Because the anisotropy of the friction coefficient affects the dynamics only marginally (although it affects the viscous component of the stress tensor), in the present simulations we set $\zeta_\parallel = \zeta$ (isotropic drag) for simplicity.

We show here that strong enough shear flow considerably speeds up the collapse kinetics because it increases the likelihood that the two ends of the chain meet. Figure 8 shows the trend of the decay rate as a function of the Weissenberg number Wi, where Wi $= \dot{\gamma}\tau_{rot,L_p}$, for three different values of L/L_p. The Weissenberg number describes the ratio between the polymer characteristic relaxation time and the time scale of the flow. Consistently with what was done in the other sections of this paper, we use the rotational diffusion time of a rod of length L_p as the polymer characteristic time. For shear flow, the characteristic time scale is given by $1/\dot{\gamma}$ [29]. When the Weissenberg number Wi is smaller than one the polymer can relax—in this case rotate over a section L_p—in the time scale of the flow, while for Wi > 1 the flow is fast with respect to the polymer relaxation. At Wi $= 0.1$, the decay rate does not change much with respect to the equilibrium value, and there is not a clear trend among the different L/L_p. At Wi $= 1$, the increase in decay rate becomes instead significant, as the average time to first contact halves; for Wi $= 10$, the effect of shear flow is completely dominating and the decay rate under the three different conditions is almost equivalent. Under shear flow, the semiflexible molecules undergo a sequence of compressions and extensions while tumbling in the plane of shear; in the compression region, the molecules tend to shrink, therefore raising the probability that two sections far apart along the chain back-
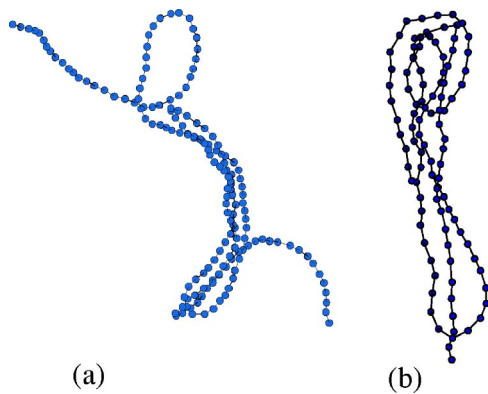
FIG. 9. (Color online) Collapsed configurations of semiflexible chains in shear flow at Wi $= 10$; (a) $L/L_p = 8$, and (b) $L/L_p = 5$.

bone come in contact. The attractive forces then trap the molecule in the partially collapsed configuration, preventing it from straightening back in the extension region.

However, the continuous tumbling of the chain and alternation of extension and compression does not allow the formation of the higher order, compact structures observed at equilibrium. In particular, the shear flow seems to inhibit the formation of the torus, which was never observed in the high shear flow simulations. Figure 9 shows two typical configurations observed in strong shear flow; while they show the basic features of the metastable racquets, the structures are less compact and do not reach the same level of energy of the equilibrium conditions.

IV. DISCUSSION

The dynamics of collapse of semiflexible molecules in bad solvent has been recently investigated in the literature. Direct, visual experimental evidence of the formation of tori and high order racquets has been obtained studying biopolymers with sufficiently large persistence lengths [13,14]. Theoretical work and Monte Carlo simulations [11,12,24] have confirmed that the torus is the stable conformation, but intermediate, metastable racquet-shaped conformations exist and are long lived. Previous Brownian Dynamics simulations in 2D [15] have firstly suggested the possible general pathways to the dynamics of collapse.

The present work provides new insights on the collapse of semiflexible chains, confirming the suggested pathways through 3D simulations, and showing the effect of the two relevant dimensionless ratios L/L_p and L_0/L_p on the kinetics of collapse. The time series of the total energy of each chain show clearly the fast transition between well-defined energy levels, corresponding to different metastable intermediate shapes, and the final, stable torus. We also showed that two possible pathways towards the stable conformation are pos-

sible: direct formation of a torus and successive folding of the chain in progressively higher order racquets. The latter one appears to be more probable for the range of parameters investigated. The decay rate of uncollapsed states for all the different conditions of the simulation can be plotted as a function of a proper combination of L/L_p and L_0/L_p. Further work is needed to confirm the validity of this empirical scaling and verify it in a wider range of parameters. In particular, this scaling does not provide a proper dependence of the decay rate from the persistence length alone, because L_p is never varied ($L_p = 20$ connector lengths for all the simulations).

We also performed simulations with different computational models, therefore confirming that the observed metastable conformations and pathways are general and do not depend on the model details. However, the kinetics, i.e., the actual value of the decay rate, can be different: in particular, for a constrained bead-rod model the kinetics of collapse appear slower, possibly due to the way the Brownian noise is projected onto the constraints.

We show preliminary results on the kinetics and pathways of collapse of semiflexible chains in shear flow. Strong enough shear flow increases the decay rate of uncollapsed states, but prevents the formation of the compact, well-defined configuration observed at rest, and seems to inhibit the formation of the torus. Based on this evidence, the fastest kinetics of condensation should be achievable by shearing the molecules initially—to promote the initial collapse—and then stopping the flow to let internal forces drive the final collapse to the compact configurations. While these results have been obtained in unbounded shear flow, future work will consider the interaction of the collapsing molecules with a solid surface, which could be attractive or repulsive for the chain. Also, a future possible direction of research includes the effect of local defects along the chain, which make the molecule locally more flexible or stiffer, as well as the dynamics of compaction when specific binding sites are induced in the chain, for example, by proteins on DNA molecules.

[1] P. G. de Gennes, *Scaling Concepts in Polymer Physics*, 1st ed. (Cornell University Press, Ithaca, 1979).

[2] R. A. Bird, C. F. Curtiss, R. C. Armstrong, and O. Hassager, *Dynamics of Polymeric Liquids*, 2nd ed. (Wiley, New York, 1987), Vol. 2.

[3] M. Doi and S. F. Edwards, *The Theory of Polymer Dynamics*, 1st ed. (Oxford University Press, Oxford, 1986).

[4] P.G. de Gennes, J. Phys. (France) Lett. **46**, 639 (1985).

[5] B. Ostrovsky and Y. Baryam, Europhys. Lett. **25**, 409 (1994).

[6] K.A. Dawson, E.G. Timoshenko, and Y.A. Kuznetsov, Physica A **236**, 58 (1997).

[7] A. Halperin and P. Goldbart, Phys. Rev. E **61**, 565 (2000).

[8] B. Chu, Q.C. Ying, and A.Y. Grosberg, Macromolecules **28**, 180 (1995).

[9] C.F. Abrams, N.K. Lee, and S.P. Obukhov, Europhys. Lett. **59**, 391 (2002).

[10] A.Y. Grosberg, Biofizika **24**, 32 (1979).

[11] V.A. Bloomfield, Biopolymers **44**, 269 (1997).

[12] H. Noguchi, S. Saito, S. Kidoaki, and K. Yoshikawa, Chem. Phys. Lett. **261**, 527 (1996).

[13] I. Baeza, P. Gariglio, L.M. Rangel, P. Chavez, L. Cervantes, C. Arguello, C. Wong, and C. Montañez, Biochemistry **26**, 6387 (1987).

[14] A.L. Martin, M.C. Davies, B.J. Rackstraw, C.J. Roberts, S. Stolnik, S.J.B. Tendler, and P.M. Williams, FEBS Lett. **480**, 106 (2000).

[15] F. Schnurr, F.C. MacKintosh, and D.R.M. Williams, Europhys. Lett. **51**, 279 (2000).

[16] H. Noguchi and K. Yoshikawa, J. Chem. Phys. **113**, 854 (2000).

[17] T. Sakaue and K. Yoshikawa, J. Chem. Phys. **117**, 6323 (2002).

[18] D.T. Hung, L.J. Marton, D.F. Deen, and R.H. Shafer, Science **221**, 368 (1983).

[19] From slender body hydrodynamics, $\zeta = 4\pi\eta_s\varepsilon$, where $\varepsilon \equiv 1/\ln(L/r)$, r is the rod radius, and $f(\varepsilon) \approx 1$ for slender rods.

[20] A.Y. Grosberg, T.T. Nguyen, and B.I. Shklovskii, Rev. Mod. Phys. **74**, 329 (2002).

[21] P.S. Grassia and E.J. Hinch, J. Fluid Mech. **308**, 255 (1996).

[22] M. Pasquali, V. Shankar, and D.C. Morse, Phys. Rev. E **64**, 020802(R) (2001).

[23] M. Pasquali and D.C. Morse, J. Chem. Phys. **116**, 1834 (2002).

[24] B. Schnurr, F. Gittes, and F.C. MacKintosh, Phys. Rev. E **65**, 061904 (2002).

[25] See EPAPS Document No. E-PLEEE8-69-073402 for movies showing two typical pathways, direct formation of a torus, and successive folding of the chain into higher order racquets. A direct link to this document may be found in the online article's HTML reference section. The document may also be reached via the EPAPS homepage (http://www.aip.org/pubservs/epaps.html) or from ftp.aip.org in the directory/epaps/. See the EPAPS homepage for more information.

[26] N. A. C. Cressie, *Statistics for Spatial Data*, 1st ed. (Wiley, New York, 1991)

[27] A. Montesi, C. Wiggins, and M. Pasquali (in preparation).

[28] D. Petera and M. Muthukumar, J. Chem. Phys. **111**, 7614 (1999).

[29] The behavior of semiflexible polymers in shear flow can be characterized also through the ratio of viscous forces induced by the flow and elastic forces due to the bending stiffness, i.e., the elasticity number $El = \dot{\gamma}\zeta L^4/(\alpha^4 k_B T L_p)$, where α is the eigenvalue of the dominant buckling eigenmode. El is related to Wi through the ratio L/L_p.